http://dx.doi.org/10.5012/bkcs.2014.35.6.1706

# Dynamics of OH Production in the Reaction of $O(^1D_2)$ with Cyclopropane

**Sungwoo Jang, Sung Il Jin, Hong Lae Kim,† Hyung Min Kim,* and Chan Ryang Park***

*†Department of Chemistry and Institute for Molecular Science and Fusion Technology, Kangwon National University, Chuncheon 200-701, Korea*
*Department of Chemistry, Kookmin University, Seoul 136-702, Korea*
**E-mail: crpark@kookmin.ac.kr (C.R. Park); hyungkim@kookmin.ac.kr (H.M. Kim)*
*Received February 11, 2014, Accepted February 14, 2014*

The $OH(X^2\Pi, \upsilon'' = 0,1)$ internal state distribution following the reaction of electronically excited oxygen atom ($O(^1D_2)$) with cyclo-$C_3H_6$ has been measured using laser-induced fluorescence, and compared with that following the reaction of $O(^1D_2)$ with $C_3H_8$. The overall characteristics of the OH internal energy distributions for both reactions were qualitatively similar. The population propensity of the $\Pi(A')$ Λ-doublet sub-level suggested that both reactions proceeded *via* an insertion/elimination mechanism. Bimodal rotational population distributions supported the existence of two parallel mechanisms for OH production, *i.e.*, statistical insertion and nonstatistical insertion. However, detailed analysis revealed that, despite the higher exoergicity of the reaction, the rotational distribution of the OH following the reaction of $O(^1D_2)$ with $C_3H_8$ was significantly cooler than that with cyclo-$C_3H_6$, especially in the vibrational ground state. This observation was interpreted as the effect of the flexibility of the insertion complex and faster intramolecular vibrational relaxation (IVR).

**Key Words :** $O(^1D_2)$, Cyclopropane, OH, Internal energy distribution, IVR

## Introduction

The reactions of electronically excited atomic oxygen, $O(^1D_2)$, with small hydrogen-containing molecules[1] have attracted a significant amount of attention owing to their importance in establishing the chemical composition and physical structure of the atmosphere, and also their fundamental interest in reaction dynamics. Thermal rate coefficients for the reactions of $O(^1D_2)$ with hydrocarbons are generally very large,[2] approaching those of gas kinetic values. The channel producing electronic ground-state OH (reaction 1) has been studied comprehensively using laser-induced fluorescence (LIF),[3] infrared chemiluminescence techniques,[4] and crossed molecular beam studies.[5] Reaction 1 is highly exothermic, releasing ~190 kJ mol$^{-1}$ for $CH_4$, and ~200-220 kJ mol$^{-1}$ for higher saturated hydrocarbons,[6] which is enough to produce vibrationally excited $OH(X^2\Pi, 0 \le \upsilon'' \le 4)$.

$$O(^1D_2) + RH \rightarrow OH(X^2\Pi) + R \quad (1)$$

Full characterization of the OH product distribution following the reaction of $O(^1D_2)$ with various hydrocarbons, *i.e.*, $CH_4$, $C_2H_6$, $C_3H_8$, and $C(CH_3)_4$, has been reported using LIF on the transitions $OH(A^2\Sigma, \upsilon' = 0, 1 \leftarrow X^2\Pi, 0 \le \upsilon'' \le 4)$, and can be summarized as follows.[7] The population of $OH(X^2\Pi, \upsilon'')$ products is broadly distributed over vibrational levels up to the energetic limit of $\upsilon'' = 4$, and extends over the available rotational levels within each $\upsilon''$. The rotational surprisals demonstrated bimodal characters and revealed significant nonlinearity in the lower vibrational levels of the heavier hydrocarbons. The product energy distributions were interpreted to reflect the roles played by two parallel mechanisms leading to the formation of OH, in which both mechanisms involved the formation of vibrationally excited insertion complexes as typified in reaction 2.

$$O(^1D_2) + RH \rightarrow ROH^{\dagger} \rightarrow R + OH(X^2\Pi) \quad (2)$$

One mechanism dominates the $O(^1D_2)/CH_4$ reaction, as well as the higher vibrational levels of OH in heavier hydrocarbons. It favors the production of the rovibrationally excited product in a manner similar to analogous reactions of $O(^1D_2)$ with substrates such as $H_2$ and HCl, and probably involves the dissociation of short-lived $ROH^{\dagger}$ prior to energy equipartition in the complex. The second mechanism leads, in the case of heavier hydrocarbons, to the production of rotationally and vibrationally cold OH. Deconvolution of the bimodal distribution based on information theoretic analysis and RRKM calculations have concluded that the production of $OH(X^2\Pi, \upsilon'' = 0)$ following the reaction of $O(^1D_2)$ with heavier hydrocarbons proceeds *via* an activated collision complex intermediate that is sufficiently long-lived to ensure the equilibration of the reaction exoergicity prior to dissociation.

For all hydrocarbons larger than $CH_4$, there are generally more exothermic channels involved in the rupture of weaker C–C bonds. The relatively small yields of OH resulting from the reactions of $O(^1D_2)$ with heavier hydrocarbons (< 5% relative to $CH_4$)[7] certainly support a mechanism in which the production of a chemically activated alcohol (reaction 2) is followed predominantly by C–C bond scission to yield products other than OH, because the C–C bond is much weaker than the C–O bond.

More recently, based on the time-resolved ultrafast LIF measurements of the OH from the reaction of $O(^1D_2)$ with

$CH_4$, Stephenson and co-workers proposed three distinguishable mechanisms for reaction 1.[8] The longest lifetime (5 ps) was associated with statistical insertion; that is, the intermediate $ROH^{\dagger}$ was sufficiently long-lived for complete intramolecular vibrational relaxation (IVR). The intermediate lifetime (0.5 ps) was attributed to nonstatistical insertion, or an insufficient lifetime for complete IVR. The shortest lifetime (0.2 ps) was assigned to abstraction on the basis of its cold rovibrational distribution.

In the present study, using LIF, the $OH(X^2\Pi, \upsilon'' = 0,1)$ internal state distributions following the reactions of $O(^1D_2)$ with $C_3H_8$ and cyclo-$C_3H_6$ were measured and compared (reactions 3 and 4).

$$O(^1D_2) + \text{cyclo-}C_3H_6 \rightarrow OH(X^2\Pi) + \text{cyclo-}C_3H_5 \quad (3)$$

$$O(^1D_2) + C_3H_8 \rightarrow OH(X^2\Pi) + C_3H_7 \quad (4)$$

As described above, the OH production channel for reaction 4 was studied up to the energetic limit using LIF.[7] Since both substrate molecules, $C_3H_8$ and cyclo-$C_3H_6$, are saturated hydrocarbons with approximately the same molecular weights, it is expected that both reactions will follow kinematically the same reaction mechanism for the production of OH. Recently, a number of reaction pathways for the reaction of $O(^1D_2)$ with cyclo-$C_3H_6$ have been observed using crossed molecular beam studies.[9,10] Interestingly enough, in addition to the insertion into the C–H bond, it has been reported that $O(^1D_2)$ inserts into the C–C bond of cyclo-$C_3H_6$, followed by the production of $H_2CO$ through long-lived complex formation, which is not generally observed for the reaction of $O(^1D_2)$ with $C_3H_8$. Another main difference between reactions 3 and 4 lies in the molecular flexibilities of the substrates. Cyclo-$C_3H_6$ has a very rigid structure with a high ring strain energy (~114 kJ/mol), while $C_3H_8$ is very flexible because large-amplitude torsional motions around the C–C single bonds are possible. The different internal energy distributions of $OH(X^2\Pi, \upsilon'' = 0,1)$ products following reactions 3 and 4 are discussed in terms of the flexibility of the intermediate collision complex in each reaction and the energy randomization rate of the initial local excitation of vibrations in the complex.

## Experimental

Pulsed production of $O(^1D_2)$ was accomplished using Nd:YAG laser (Spectra Physics, DCR-11) with photodissociation of $O_3$ at 266 nm. The $OH(X^2\Pi, \upsilon'', N'', f'', \lambda'')$ products were monitored by LIF using the (0,0) and (1,1) bands of the $A^2\Sigma$-$X^2\Pi$ transitions in the 306-324 nm region. The Nd:YAG (Spectra Physics GCR-150)-pumped dye laser (Lumonics HD500) used to excite the $A^2\Sigma$-$X^2\Pi$ transition was fired approximately 100 ns after the photolysis laser. Under typical experimental conditions ($P_{RH}$ = 50 mTorr, $P_{O3}$, = 10 mTorr, $P_{He}$ = 90 mTorr), an OH molecule undergoes an average of ~0.5 gas kinetic collisions in that time.

The fluorescence of $A^2\Sigma, \upsilon' = 0, 1 \rightarrow X^2\Pi, \upsilon'' = 0, 1$ near 310 nm was observed with a filtered (UG11) high-gain photomultiplier tube (PMT; Hamamatsu, R2059). The excitation laser power was kept as low as possible to prevent saturation. Variations in photolysis and probe laser signal intensities were monitored continuously, and the LIF signals were corrected accordingly. The electronic signal from the PMT was then sampled with a boxcar (EG&G 4161A, 4121B) and recorded by a laboratory computer system. All equipment was controlled and synchronized using the LabVIEW program.

No correction was made for the electronic quenching of the $A^2\Sigma$ state in collisions with RH in the absence of specific information about rotational level-dependent quenching rate constants. Under the present experimental conditions, these corrections were estimated to be relatively small and fall within the limit of experimental error.[11,12] The photodissociation of $O_3$ at 266 nm produces ~10% of the atomic oxygen in the ground electronic state, $O(^3P_J)$, which can have large translational energies. The rate coefficient of the $O(^3P_J)$ reaction with hydrocarbon is, however, at most $10^{-7}$ that of the $O(^1D_2)$ reaction at room temperature.[13] For this reason, the contribution of $O(^3P_J)$ as a source of the OH product was ignored.

All gas solutions were prepared and allowed to mix in a grease-free glass flow-cell through needle valve. The preparation and treatment of $O_3$ and He have been previously described.[7] Cyclo-$C_3H_6$ (Aldrich, 99.9%) and $C_3H_8$ (Aldrich, 99.9%) were used as received.

## Results and Discussion

The LIF spectra observed following reactions 3 and 4 (Figure 1) display the characteristic $OH(A^2\Sigma^+ \leftarrow X^2\Pi)$ transi-

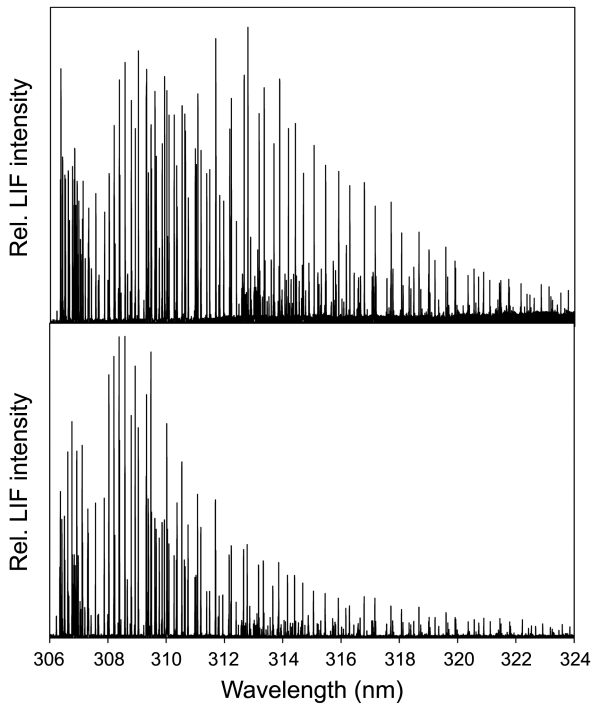


**Figure 1.** Merged LIF spectrum of the OH product arising from (upper) $O(^1D_2)$ + cyclo-$C_3H_6$ → $OH(X^2\Pi)$ + cyclo-$C_3H_5$, (lower) $O(^1D_2)$ + $C_3H_8$ → $OH(X^2\Pi)$ + $C_3H_7$ obtained under the experimental conditions described in the text.

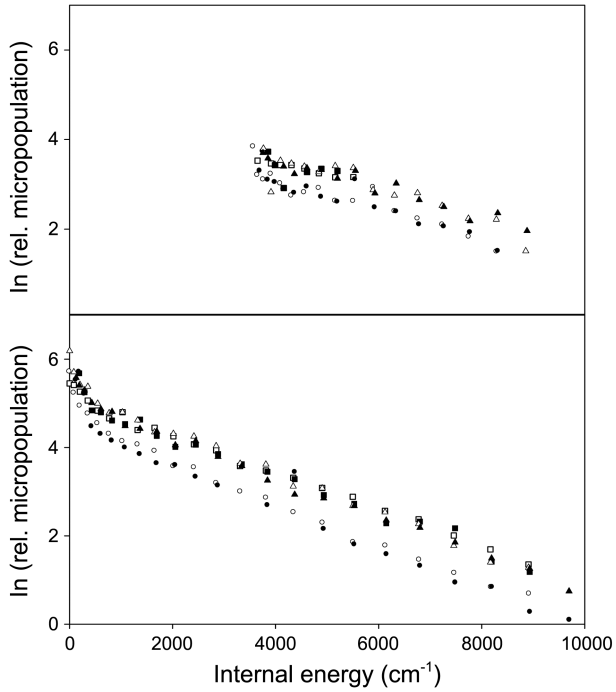


**Figure 2.** Micropopulation distributions of the OH products derived from experimental spectrum for $O(^1D_2)$ + cyclo-$C_3H_6$; $P_{11}$(□), $P_{22}$(■), $Q_{11}$(○), $Q_{22}$(●), $R_{11}$(△), $R_{22}$(▲).

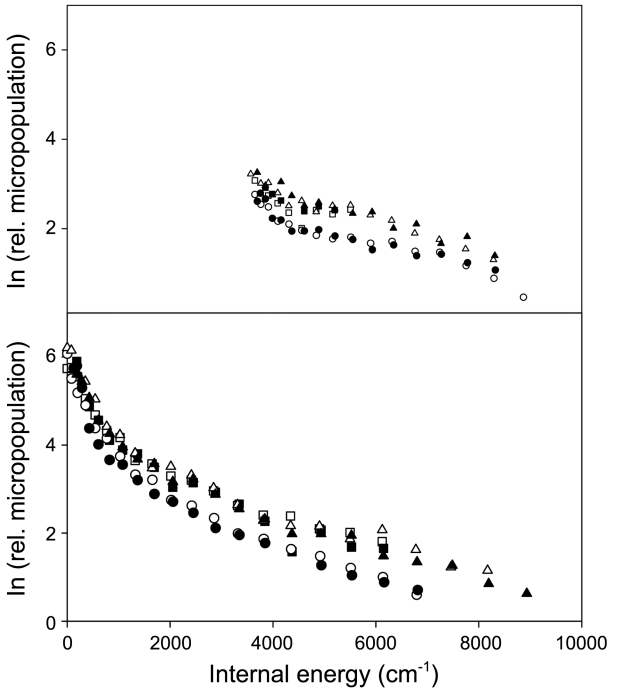


**Figure 3.** Micropopulation distributions of the OH products derived from experimental spectrum for $O(^1D_2)$ + $C_3H_8$; $P_{11}$(□), $P_{22}$(■), $Q_{11}$(○), $Q_{22}$(●), $R_{11}$(△), $R_{22}$(▲).

tions[14] corresponding to the absorption by diatomic molecules formed in υ" = 0 and 1. A more extensive population of OH($X^2\Pi$, υ" = 0) from reaction 3 is clearly seen from Figure 1; the R-band head of the (0,0) band begins at *ca.* 306 nm and that of the (1,1) band begins at *ca.* 312 nm. Conversion of the measured LIF signal $S$ to the state-resolved OH($X^2\Pi$) population requires correction for variation in the intensities of both the photolysis and probe lasers, $I_{photo}$ and $I_{probe}$, as well as the accurate values of the Einstein coefficients, $B_{\upsilon'',J''}^{\upsilon',J'}$, for the stimulated absorption. Tabulated values of $B_{\upsilon'',J''}^{\upsilon',J'}$ provided by Crosley were used throughout.[15] The linearity of the LIF measurements was confirmed by comparing the relative intensities of the satellite and main branch transitions that probe the same level of OH($X^2\Pi$, $\upsilon''$, $N''$, $f''$, $\lambda''$).

$$P(\upsilon'', N'', f'', \lambda'') \propto S/I_{photo}\, I_{probe} B_{\upsilon'',J''}^{\upsilon',J'} \quad (5)$$

Micropopulation distributions (population divided by the rotational degeneracy, $2J''+1$) for the OH($X^2\Pi$) product arising from the $O(^1D_2)$/cyclo-$C_3H_6$ and $O(^1D_2)$/$C_3H_8$ reactions are displayed in Figure 2 and Figure 3, respectively. On the whole, the results reported previously[7] for the internal energy distributions of the OH product following reaction 4 were satisfactorily reproduced. The micropopulation distributions for OH products indicated that the gross features of the OH distributions following reactions 3 and 4 closely resembled each other. Closer inspection of Figure 2 and Figure 3, however, revealed that the rotational distribution of OH($X^2\Pi$, υ" = 0) from reaction 4 was relatively more relaxed compared with that from reaction 3, especially in the low-$J$ region. However, reaction 4 is more exothermic than reaction 3 by as much as ~34 kJ/mol, amounting to *ca.* 20% of the total exothermicity. This seemingly contradictory observation is reserved for the discussion.

Spin-orbit coupling produces two fine structure states, $f_1$ and $f_2$, which correspond to $X^2\Pi_{3/2}$ and $X^2\Pi_{1/2}$, respectively. The $f_1$ state is probed by the $P_{11}$ and $Q_{11}$ transitions, while the $f_2$ is probed by the $P_{22}$ and $Q_{22}$. Analysis of the spectra revealed that the ratio of the fine structure state micropopulations summed over all the accessible rotational levels was about the same within experimental error for the two vibrational states, $P(^2\Pi_{3/2})/P(^2\Pi_{1/2}) = 1.1 \pm 0.11$ for OH($X^2\Pi$, υ" = 1), and $1.3 \pm 0.13$ for OH($X^2\Pi$, υ" = 0) (Table 1). Thus, for the reactions examined here, there was no significant difference between the populations of the fine structure levels in υ" = 1, and there was a slight difference favoring the production of the lower level ($^2\Pi_{3/2}$) in υ" = 0. This observation is in contrast to the previously reported pronounced preferential population of the lower-lying $f_1$ state (about two times larger population) of the OH product produced in the reaction of ground state atomic oxygen ($O(^3P_J)$) with hydrocarbons,[16] a reaction that is known to proceed *via* a direct abstraction mechanism.

Two Λ-doublet fine structure states arise from orbital and rotational angular momenta coupling, namely $\Pi(A')$ and $\Pi(A'')$. The former corresponds to the orientation of the half-filled π orbital in the plane of the OH rotation in the limit of high rotational states, while the latter corresponds to the orientation perpendicular to that plane. Preferential production of $\Pi(A')$ in the $O(^1D_2)/H_2$ reaction, for example, has been ascribed to the establishment of oriented product rotation during the dissociation of the planar HOH intermediate

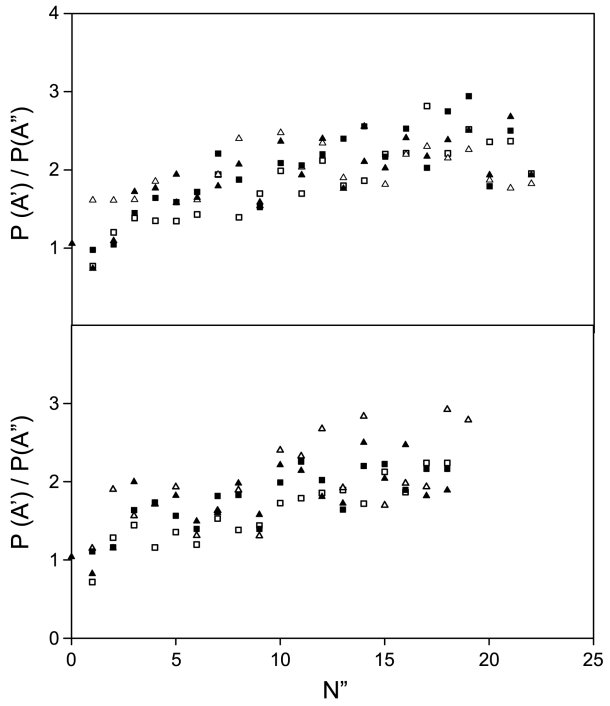


**Figure 4.** Dependence of Λ-doublet population ratios $P(A')/P(A")$ upon rotational state in (upper) OH($X^2\Pi$, υ" = 0) from O($^1D_2$) + cyclo-$C_3H_6$, and (lower) OH($X^2\Pi$, υ" = 0) from O($^1D_2$) + $C_3H_8$; $P_{11}/Q_{11}$ (□), $R_{11}/Q_{11}$ (△), $P_{22}/Q_{22}$ (■), $R_{22}/Q_{22}$ (▲).

complex.[17] Direct abstractions, on the other hand, do not result in the preferential formation of either Λ-doublet state.

The OH formed in reaction 3 displayed a characteristic propensity for the production of the $\Pi(A')$ Λ-doublet sublevel, as observed in the OH product of reaction 4 (Figure 2 and Figure 3). The values of $\Pi(A')/\Pi(A")$ in Table 1 were estimated by averaging over all the observed $J$ levels. This ratio is known to increase as $J$ increases.[18] Dependence of the Λ-doublet population ratios $P(A')/P(A")$ on the rotational state in OH($X^2\Pi$, υ" = 0) are plotted in Figure 4. Preferential population of the $\Pi(A')$ state observed in reaction 3 demonstrates that the half-filled π orbital of the OH radical lies preferentially oriented in its rotational plane.[3] This, in turn, implies that OH production results from the dissociation of a cyclo-$C_3H_5OH^\dagger$ complex, with the nascent π orbital remaining in the plane containing the C–O bond.

It has been reported that in the reaction of O($^1D_2$) with $CH_4$, $C_2H_6$, $C_3H_8$, and $C(CH_3)_4$, the degree of preferential orientation of OH in the plane of product rotation depends on the size of the substrate.[7] The population ratio of $P[\Pi(A')]/P[\Pi(A")]$ revealed that the OH produced from the O($^1D_2$)/$CH_4$ reaction displayed the greatest preference, while that from O($^1D_2$)/$C(CH_3)_4$ showed the least. That seems reasonable in view of the increasing complexity of the $ROH^\dagger$ intermediate arising from the O($^1D_2$) insertion into larger substrates and hence, the more poorly defined plane of dissociation. Increased Λ-doublet selectivity of the OH from reaction 3 compared with that from reaction 4 (Table 1) may reflect the strengthening of this planarity constraint in the cyclo-$C_3H_5OH$ complex due to the planar geometry of the cyclopropane moiety. The evidence presented here certainly suggests that the reaction, O($^1D_2$)/cyclo-$C_3H_6$ or O($^1D_2$)/$C_3H_8$, is dominated by a mechanism in which O($^1D_2$) inserts into a C–H bond to yield a chemically activated alcohol as typified in reaction 2, which then dissociates to yield either OH or a pair of fragments that could not be detected in the present experiments. The reaction of C–C rupture is heavily favored because the C–C bond is weaker than the C-O bond by ~25 kJ/mol.

Vibrational populations are estimated by summing over the observed rotational distributions in each vibrational level. Due to the predissociation at higher rotational levels ($J' > 22.5$ and 13.5 at $\upsilon' = 0$ and 1, respectively) of the OH $A^2\Sigma^+$ caused by the crossing of the $^4\Sigma^-$ state, populations of the highest rotational levels were estimated by extrapolating the linear rotational surprisals up to the thermochemical limit of the reaction. To calculate the rotational surprisals, $I(f_r|f_\upsilon) = -\ln[P(f_r|f_\upsilon)/P^0(f_r|f_\upsilon)]$, statistical prior distributions of the OH products, $P^0(f_r|f_\upsilon)$, were obtained using the method presented elsewhere.[7] Table 1 reveals that, despite the higher reaction exothermicity, reaction 4 exhibits a cooler vibrational distribution ($P(\upsilon" = 1)/P(\upsilon" = 0) = 0.22$) compared to reaction 3 ($P(\upsilon" = 1)/P(\upsilon" = 0) = 0.30$) (*vide infra*).

The rotational surprisals presented in Figure 5 and Figure 6 vividly demonstrate the bimodal character in the rotational distributions characterizing the OH($X^2\Pi$) product of the O($^1D_2$) reaction with $C_3H_8$ and cyclo-$C_3H_6$, especially in the ground vibrational state. It has been reported[7] that rotational surprisals for the reaction of O($^1D_2$) with heavier hydrocarbons, *i.e.*, $C_2H_6$, $C_3H_8$, and $C(CH_3)_4$, exhibit significant nonlinearities in the lower vibrational levels, which agrees with our results. The bimodal rotational surprisals, which can be deconvoluted into two apparently linear unimodal components, *i.e.*, high-$J$ and low-$J$ components, strongly imply that both reactions produce the OH product in its lower vibrational levels *via* two distinct channels.[7]

The higher-lying rotational levels with positive slopes, $dI(f_r|f_\upsilon)/dg_R$ where $g_R = f_r/(1 - f_\upsilon)$, indicate a much higher production of the rotational levels in the high-$J$ component of the distribution than statistically expected. Such values are often associated with products formed in the dissociation of highly energized intermediates like $HOH^\dagger$ in the reaction

**Table 1.** Observed OH population distributions following the reaction of O($^1D_2$) with cyclo-$C_3H_6$ and $C_3H_8$

| | $P(A')/P(A")$ | | $P(^2\Pi_{3/2}) / P(^2\Pi_{1/2})$ | | $P(\upsilon"=1)/P(\upsilon"=0)$ |
|---|---|---|---|---|---|
| | υ"=0 | υ"=1 | υ"=0 | υ"=1 | |
| O($^1D_2$) + cyclo-$C_3H_6$ | 1.7 ± 0.17 | 1.5 ± 0.30 | 1.3 ± 0.13 | 1.1 ± 0.22 | 0.30 ± 0.03 |
| O($^1D_2$) + $C_3H_8$ | 1.3 ± 0.13 | 1.5 ± 0.30 | 1.3 ± 0.13 | 1.1 ± 0.22 | 0.22 ± 0.02 |

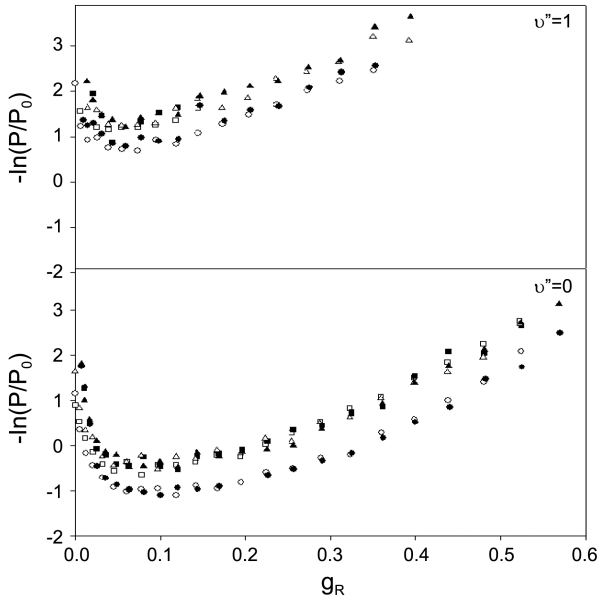


**Figure 5.** Rotational surprisals of OH($X^2\Pi$, υ") produced from the $O(^1D_2)$/cyclo-$C_3H_6$ reaction that have been derived from the statistical prior [$P^0(f_r|f_v)$] and the experimental distributions displayed in Figure 2, with the abscissa defined as $g_R = f_r/(1 - f_v)$; $P_{11}$(□), $P_{22}$ (■), $Q_{11}$(○), $Q_{22}$(●), $R_{11}$(△), $R_{22}$(▲).

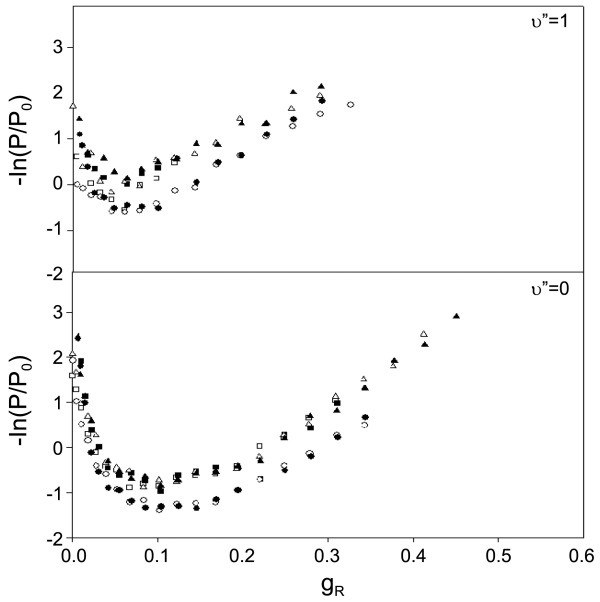


**Figure 6**. Rotational surprisals of OH($X^2\Pi$, υ") produced from the $O(^1D_2)$/$C_3H_8$ reaction that have been derived from the statistical prior [$P^0(f_r|f_v)$] and the experimental distributions displayed in Figure 3, with the abscissa defined as $g_R = f_r/(1 - f_v)$; $P_{11}$(□), $P_{22}$(■), $Q_{11}$ (○), $Q_{22}$(●), $R_{11}$(△), $R_{22}$(▲).

of $O(^1D_2)$ with $H_2$, and reflect the effective conversion of R–O–H bending of the highly energized collision complex into OH rotation. That, in turn, suggests that the high-*J* component may arise from the dissociation of an $ROH^\dagger$ intermediate prior to the equilibration of available reaction exoergicity in that complex through intramolecular energy transfer among available modes. On the other hand, the low-*J* component, which nearly vanishes in the rotational distribution of OH above υ" = 1 as reported in previous work,[7] appears to be nearly thermal in nature. In the case of a relatively large substrate, the resulting collision complex, $ROH^\dagger$, would be expected to be long-lived and the available reaction exoergicity would be randomized as to preclude the vibrational excitation of the OH product following dissociation. This intuitive view supports the lack of significant vibrational excitation of OH following the reaction of $O(^1D_2)$ with large alkanes, as well as the much cooler rotational distribution of OH in its ground vibrational level.

The evidence presented thus far certainly suggests that the $O(^1D_2)$/cyclo-$C_3H_6$ or $O(^1D_2)$/$C_3H_8$ reaction is dominated by a mechanism in which $O(^1D_2)$ inserts into a C–H bond to yield a chemically activated alcohol, which then dissociates to yield OH. The bimodal rotational product population distribution provides significant support for the existence of two parallel mechanisms for the OH product, which is in accord with Stephenson's mechanisms mentioned in the previous section; *i.e.*, statistical insertion and nonstatistical insertion.[8]

As pointed out previously, the micropopulations in Figure 2 and Figure 3 show that the rotational distribution of OH($X^2\Pi$, υ" = 0) following reaction 4 is cooler than that following reaction 3, especially at lower-lying rotational levels. The difference in the rotational distributions of OH between the two reactions can be seen more vividly in Figure 7, where relative rotational populations of OH($X^2\Pi$, υ" = 0) following both reactions are plotted as a function of rotational quantum number, $N''$, and spin-orbit states, $f_1$ and $f_2$. The rotational degeneracy, $2J'' + 1$, is counted to estimate the population, and the total population of OH($X^2\Pi$, υ" = 0) for each reaction is normalized for comparison. Despite the higher exothermicity of reaction 4 (~34 kJ/mol), the rotational distribution of OH($X^2\Pi$, υ" = 0) following reaction 4 shows a more pronounced rotational relaxation compared with that following reaction 3. The reaction exothermicity and maximum collision energy available for each reaction are presented in Table 2. Collision energies for both reactions are estimated to be similar, since the mass difference between $C_3H_8$ and cyclo-$C_3H_6$ is only two amu.

According to previous discussions, the low-*J* component of OH, especially in its lowest vibrational level, is produced from the collision complex $ROH^\dagger$ that is sufficiently long-lived to ensure the equilibration of the reaction exoergicity prior to dissociation, or intramolecular vibrational relaxation (IVR). Then, this argument strongly implies that the rate of intramolecular vibrational relaxation of cyclo-$C_3H_5OH^\dagger$ is

**Table 2.** Reaction exothermicity and maximum collision energy available for the reaction: $O(^1D_2) + RH \rightarrow OH(X^2\Pi) + R$

| RH | $-\Delta H$(kJ/mol) | $E_{coll}$ (kJ/mol) | $E_{avail}$ (kJ/mol) |
|---|---|---|---|
| cyclo-$C_3H_6$ | 175 | 29 | 204 |
| $C_3H_8$ | 200 (*n*-$C_3H_7$) | 29 | 229 |
| | 218 (*i*-$C_3H_7$) | 29 | 247 |

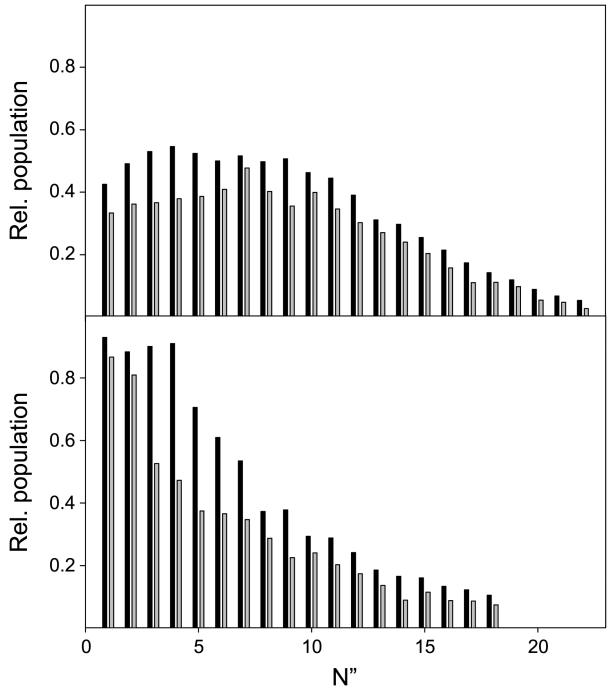


**Figure 7.** Relative rotational populations of the OH($X^2\Pi$, υ" = 0) products as a function of rotational quantum number, *N"*, and spin-orbit state, $f_1$ (solid) and $f_2$ (shaded); (upper) O($^1D_2$) + cyclo-$C_3H_6$; (lower) O($^1D_2$) + $C_3H_8$. The total population of OH($X^2\Pi$, υ" = 0) for each reaction is normalized for comparison.

slower than that of *n*-$C_3H_7OH^\dagger$ or *i*-$C_3H_7OH^\dagger$, which, in turn, indicates that cyclo-$C_3H_5OH^\dagger$ has a longer lifetime, at least in the context of IVR.

Even though IVR is conceptually very simple, experimental and theoretical efforts are still in progress to understand and predict IVR phenomena. However, empirical evidence has shown that molecular flexibility plays an important role in accelerating IVR through large-amplitude vibrational modes.[19,20] Large-amplitude methyl rotor motion and other large-amplitude torsional modes, such as around single C–O and C–C bonds, are known to enhance IVR. Furthermore, it has been pointed out that molecular flexibility can give rise to substantial low- and high-order couplings that may enhance the rate of intramolecular relaxation.

Significant evidence has been accumulated regarding the accelerating effect of a single methyl rotor substituent on IVR, and one example includes a study of the IVR rate of C–H stretching by comparing *p*-fluorotoluene and *p*-difluorobenzene.[21] The results indicated a remarkable increase in IVR rates upon methyl group substitution. The coupling between methyl rotation and low-frequency ring modes is known to be important for the promotion of the vibrational state mixing.[22,23] Moreover, aliphatic methyl internal rotation in combination with another large-amplitude modes, may play a role in enhancing IVR even if, by itself, it is generally less effective than other types of molecular flexibility. For skeletal torsion as an IVR accelerator, the effects of centers of flexibility (COF) on IVR state mixing have been reported. A particularly relevant example of this effect was published using comparative studies of 1-butene and *trans*-2-butene.[24] Both species are isomeric and have the same vibrational degrees of freedom. The structural difference between these two molecules is that the carbon chain in 1-butene is floppy with a low barrier to C–C–C torsional isomerization, whereas *trans*-2-butene is essentially rigid due to the central double bond. This modification resulted in a dramatic change in their high-resolution jet-cooled spectra. The presence of a low-barrier C–C–C torsional mode in floppy 1-butene was interpreted to bring about rotationally induced IVR state mixing not present in rigid *trans*-2-butene. In other words, the proximity of a prepared C–H vibration to a center of flexibility is associated with accelerated IVR.

Even though the experimental evidence regarding IVR rates discussed above were obtained primarily from CH- or OH-stretch IVR dynamics, this simple picture can potentially be applied to collision complexes presented in this work. Initial local vibrational excitation of the collision complex caused by the insertion of O($^1D_2$) into a C–H bond may comprise the R–O–H bending and OH-stretching motions, which, in turn, are converted to the rotational and vibrational excitation of OH diatomic products following dissociation. The structural difference between the insertion complexes studied in this work is essentially the same as the case of 1-butene and *trans*-2-butene mentioned above. The insertion of O($^1D_2$) into a C–H bond in reaction 4 can produce two isomers, namely *n*-$C_3H_7OH$ and *i*-$C_3H_7OH$. The carbon chain in *n*-$C_3H_7OH$ is floppy with a low barrier to C–C–C torsional isomerization, whereas the framework of cyclo-$C_3H_5OH$ produced from reaction 3 is essentially rigid due to the strictly planar character of the cyclopropyl ring. On the other hand, the main structural difference between *i*-$C_3H_7OH$ (reaction 4) and cyclo-$C_3H_5OH$ (reaction 3) is two additional methyl rotors in *i*-$C_3H_7OH$, which may also play an additional role in enhancing IVR. Less vibrational excitation of OH following reaction 4 ($P$(υ" = 1)/$P$(υ" = 0) = 0.22) than that following reaction 3 ($P$(υ" = 1)/$P$(υ" = 0) = 0.30) despite the higher exothermicity could also be interpreted as faster IVR in intermediate insertion complexes in reaction 4.

## Conclusion

The present work reports the OH($X^2\Pi$, υ" = 0, 1) internal state distributions following the reaction of O($^1D_2$) with cyclo-$C_3H_6$ and $C_3H_8$ using LIF. Both reactions showed qualitatively similar internal energy distributions for the OH products as expected. The propensity for the population of the $\Pi$(A′) Λ-doublet sublevel suggests that the O($^1D_2$)/cyclo-$C_3H_6$ or $C_3H_8$ reaction is dominated by a mechanism in which O($^1D_2$) inserts into a C–H bond to yield a chemically activated alcohol, which then dissociates to yield OH. Bi-modal rotational distributions support the existence of two parallel mechanisms for OH production. One mechanism is statistical insertion, *i.e.*, sufficiently long lifetime of the intermediate $ROH^\dagger$ for complete IVR, and the other is nonstatistical insertion, *i.e.*, insufficient lifetime for complete IVR. As pointed out in the introduction, the present work

was designed to elucidate the effect of the flexibility of the substrate on the internal energy distributions of the diatomic OH product. Despite the higher exothermicity of the reaction, the rotational and vibrational distributions of OH following the reaction of $O(^1D_2)$ with $C_3H_8$ were significantly cooler than those with cyclo-$C_3H_6$. This experimental observation was interpreted as the acceleration of IVR due to the presence of large-amplitude modes in the complexes, *i.e.*, the C–C–C skeletal and methyl torsions in the insertion complexes intermediating the $O(^1D_2)/C_3H_8$ reaction.

**Acknowledgments.** This work was financially supported by the Korea Science and Engineering Foundation (Grant No. R01-2003-000-10886-0), partly by the research program of Kookmin University in Korea.

## References

1. (a) Luntz, A. C.; Schinke, R.; Lester, W. A., Jr.; Gunthard, H. H. *J. Chem. Phys.* **1979**, *70*, 5908. (b) Smith, G. K.; Butler, N. E. *J. Chem. Phys.* **1980**, *73*, 2243. (c) Butler, J. E.; MacDonald, R. G.; Donaldson, D. J.; Sloan, J. *J. Chem. Phys. Lett.* **1983**, *95*, 183. (d) Aker, P. M.; Sloan, J. J. *J. Chem. Phys.* **1986**, *85*, 1412. (e) Aker, P. M.; Obrien, J.; Parsons, J. M.; Sloan, J. J. *Can. J. Chem.* **1986**, *64*, 2315. (f) Goldfield, E. M.; Wiesenfeld, J. R. *J. Chem. Phys.* **1990**, *93*, 1030. (g) Comes, F. J.; Gericke, K. H.; Manz, J. *J. Chem. Phys.* **1981**, *75*, 2853. (h) Park, C. R.; Wiesenfeld, J. R. *Chem. Phys. Lett.* **1989**, *163*, 230.
2. *CRC Handbook of Bimolecular and Termolecular Gas Reactions*; Kerr, J. A., Ed.; Chemical Rubber: Cleveland, 1981.
3. Luntz, A. C. *J. Chem. Phys.* **1980**, *73*, 1143.
4. Aker, P. M.; Obrien, J. J. A.; Sloan, J. J. *J. Chem. Phys.* **1986**, *84*, 745.
5. Casavecchia, P.; Buss, R. J.; Sibener, S. J.; Lee, Y. T. *J. Chem. Phys.* **1980**, *73*, 6351.
6. Berkowitz, J.; Ellison, G. B.; Gutman, D. *J. Phys. Chem.* **1994**, *98*, 2744.
7. Park, C. R.; Wiesenfeld, J. R. *J. Chem. Phys.* **1991**, *95*, 8166.
8. (a) van Zee, R. D.; Stephenson, J. C.; Casassa, M. P. *Chem. Phys. Lett.* **1994**, *223*, 167. (b) van Zee, R. D.; Stephenson, J. C. J. *Chem. Phys.* **1995**, *102*, 6946. (c) Miller, C. C.; van Zee, R. D.; Stephenson, J. C. J. *Chem. Phys.* **2001**, *114*, 1214.
9. Shu, J.; Lin, J. J.; Wang, C. C.; Lee, Y. T.; Yang, X.; Nguyen, T. L.; Mebel, A. M. *J. Chem. Phys.* **2001**, *115*, 7.
10. Wang, C. C.; Shu, J.; Lin, J. J.; Lee, Y. T.; Yang, X.; Nguyen, T. L.; Mebel, A. M. *J. Chem. Phys.* **2002**, *116*, 8292.
11. Doncaster, A. M.; Walsh, R. *J. Chem. Soc., Faraday Trans I* **1979**, *75*, 1126.
12. Doncaster, A. M.; Walsh, R. *Int. J. Chem. Kinet.* **1981**, *13*, 503.
13. Herron, J. T.; Huie, R. E. *J. Phys. Chem.* **1974**, *2*, 467.
14. Moor, E. A.; Richards, W. G. *Phys. Scr.* **1971**, *3*, 223.
15. Luque, J.; Crosley, D. R. *LIFBASE: Database and Spectral Simulation Program (Version 1.5)*; SRI International Report MP 99-009, 1999.
16. Andresen, P.; Luntz, A. C. *J. Chem. Phys.* **1980**, *72*, 5842.
17. Butler, J. E.; Jursich, G. M.; Watson, I. A.; Wiesenfeld, J. R. *J. Chem. Phys.* **1986**, *84*, 5363.
18. Andresen, P.; Rothe, E. W. *J. Chem. Phys.* **1985**, *82*, 3634.
19. Bethardy, G. A.; Wang, X.; Perry, D. S. *Can. J. Chem.* **1994**, *72*, 652.
20. Nesbitt, D. J.; W. Field, Robert *J. Phys. Chem.* **1996**, *100*, 12735.
21. (a) Parmenter, C. S.; Stone, B. M. *J. Chem. Phys.* **1986**, *84*, 4710. (b) Moss, D. B.; Parmenter, C. S.; Ewing, G. E. *J. Chem. Phys.* **1987**, *86*, 51. (c) Zhao, Z.-Q.; Parmenter, C. S.; Moss, D. B.; Bradley, A. J.; Knight, A. E. W.; Owens, K. G. *J. Chem. Phys.* **1992**, *96*, 6362. (d) Covelskie, R. A.; Dolson, D. A.; Parmenter, C. S. *J. Phys. Chem.* **1985**, *89*, 645. (e) Moss, D. B.; Parmenter, C. S. *J. Chem. Phys.* **1993**, *98*, 6897. (f) Timbers, P. J.; Parmenter, C. S.; Moss, D. B. *J. Chem. Phys.* **1994**, *100*, 1028.
22. Martens, C. C.; Reinhardt, W. P. *J. Chem. Phys.* **1990**, *93*, 5621.
23. Tan, X.-Q.; Majewski, W. A.; Plusquellic, D. F.; Pratt, D. W. *J. Chem. Phys.* **1991**, *94*, 7721.
24. McIlroy, A.; Nesbitt, D. J. *J. Chem. Phys.* **1994**, *101*, 3421.